Measurements of the T2K neutrino beam properties using the INGRID on-axis near detector

K. Abe [aw], N. Abgrall [p], Y. Ajima [r,6], H. Aihara [av], J.B. Albert [m], C. Andreopoulos [au], B. Andrieu [ak], M.D. Anerella [f], S. Aoki [aa], O. Araoka [r,6], J. Argyriades [p], A. Ariga [c], T. Ariga [c], S. Assylbekov [k], D. Autiero [af], A. Badertscher [o], M. Barbi [an], G.J. Barker [bd], G. Barr [aj], M. Bass [k], M. Batkiewicz [q], F. Bay [c], S. Bentham [ac], V. Berardi [v], B.E. Berger [k], I. Bertram [ac], M. Besnier [n], J. Beucher [h], D. Beznosko [ah], S. Bhadra [bh], F.d.M. Blaszczyk [h], J. Blocki [q], A. Blondel [p], C. Bojechko [ba], J. Bouchez [2], S.B. Boyd [bd], A. Bravar [p], C. Bronner [n], D.G. Brook-Roberge [e], N. Buchanan [k], H. Budd [ao], D. Calvet [h], S.L. Cartwright [ar], A. Carver [bd], R. Castillo [s], M.G. Catanesi [v], A. Cazes [af], A. Cervera [t], C. Chavez [ad], S. Choi [aq], G. Christodoulou [ad], J. Coleman [ad], G. Collazuol [x], W. Coleman [ae], K. Connolly [be], A. Curioni [o], A. Dabrowska [q], I. Danko [al], R. Das [k], G.S. Davies [ac], S. Davis [be], M. Day [ao], G. De Rosa [w], J.P.A.M. de André [n], P. de Perio [ay], T. Dealtry [aj,au], A. Delbart [h], C. Densham [au], F. Di Lodovico [am], S. Di Luise [o], P. Dinh Tran [n], J. Dobson [u], U. Dore [y], O. Drapier [n], F. Dufour [p], J. Dumarchez [ak], S. Dytman [al], M. Dziewiecki [bc], M. Dziomba [be], S. Emery [h], A. Ereditato [c], J.E. Escallier [f], L. Escudero [t], L.S. Esposito [o], M. Fechner [m,h], A. Ferrero [p], A.J. Finch [ac], E. Frank [c], Y. Fujii [r,6], Y. Fukuda [ag], V. Galymov [bh], G.L. Ganetis [f], F.C. Gannaway [am], A. Gaudin [ba], A. Gendotti [o], M. George [am], S. Giffin [an], C. Giganti [s], K. Gilje [ah], A.K. Ghosh [f], T. Golan [bg], M. Goldhaber [2], J.J. Gomez-Cadenas [t], S. Gomi [ab], M. Gonin [n], N. Grant [ac], A. Grant [at], P. Gumplinger [az], P. Guzowski [u], A. Haesler [p], M.D. Haigh [aj], K. Hamano [az], C. Hansen [t,3], D. Hansen [al], T. Hara [aa], P.F. Harrison [bd], B. Hartfiel [ae], M. Hartz [bh,ay], T. Haruyama [r,6], T. Hasegawa [r,6], N.C. Hastings [an], A. Hatzikoutelis [ac], K. Hayashi [r,6], Y. Hayato [aw], C. Hearty [e,6], R.L. Helmer [az], R. Henderson [az], N. Higashi [r,6], J. Hignight [ah], A. Hillairet [ba], E. Hirose [r,6], J. Holeczek [as], S. Horikawa [o], A. Hyndman [am], A.K. Ichikawa [ab], K. Ieki [ab], M. Ieva [s], M. Iida [r,6], M. Ikeda [ab], J. Ilic [au], J. Imber [ah], T. Ishida [r,6], C. Ishihara [ax], T. Ishii [r,6], S.J. Ives [u], M. Iwasaki [av], K. Iyogi [aw], A. Izmaylov [z], B. Jamieson [bf], R.A. Johnson [j], K.K. Joo [i], G.V. Jover-Manas [s], C.K. Jung [ah], H. Kaji [ax], T. Kajita [ax], H. Kakuno [av], J. Kameda [aw], K. Kaneyuki [2], D. Karlen [ba,az], K. Kasami [r,6], I. Kato [az], H. Kawamuko [ab], E. Kearns [d], M. Khabibullin [z], F. Khanam [k], A. Khotjantsev [z], D. Kielczewska [bb], T. Kikawa [ab], J. Kim [e], J.Y. Kim [i], S.B. Kim [aq], N. Kimura [r,6], B. Kirby [e], J. Kisiel [as], P. Kitching [a], T. Kobayashi [r,6], G. Kogan [u], S. Koike [r,6], A. Konaka [az], L.L. Kormos [ac], A. Korzenev [p], K. Koseki [r,6], Y. Koshio [aw], Y. Kouzuma [aw], K. Kowalik [b], V. Kravtsov [k], I. Kreslo [c], W. Kropp [g], H. Kubo [ab], J. Kubota [ab], Y. Kudenko [z], N. Kulkarni [ae], Y. Kurimoto [ab], R. Kurjata [bc], T. Kutter [ae], J. Lagoda [b], K. Laihem [ap], M. Laveder [x], K.P. Lee [ax], P.T. Le [ah], J.M. Levy [ak], C. Licciardi [an], I.T. Lim [i], T. Lindner [e], R.P. Litchfield [bd,ab], M. Litos [d], A. Longhin [h], G.D. Lopez [ah], P.F. Loverre [y], L. Ludovici [y], T. Lux [s], M. Macaire [h], K. Mahn [az], Y. Makida [r,6], M. Malek [u], S. Manly [ao], A. Marchionni [o], A.D. Marino [j], A.J. Marone [f], J. Marteau [af], J.F. Martin [ay,4], T. Maruyama [r,6], T. Maryon [ac], J. Marzec [bc], P. Masliah [u], E.L. Mathie [an], C. Matsumura [ai], K. Matsuoka [ab], V. Matveev [z], K. Mavrokoridis [ad], E. Mazzucato [h], N. McCauley [ad], K.S. McFarland [ao], C. McGrew [ah], T. McLachlan [ax], M. Messina [c], W. Metcalf [ae], C. Metelko [au], M. Mezzetto [x], P. Mijakowski [b], C.A. Miller [az], A. Minamino [ab], O. Mineev [z], S. Mine [g], A.D. Missert [j], G. Mituka [ax], M. Miura [aw], K. Mizouchi [az], L. Monfregola [t], F. Moreau [n], B. Morgan [bd], S. Moriyama [aw], A. Muir [at], A. Murakami [ab], J.F. Muratore [f], M. Murdoch [ad], S. Murphy [p], J. Myslik [ba], N. Nagai [ab], T. Nakadaira [r,6], M. Nakahata [aw], T. Nakai [ai], K. Nakajima [ai], T. Nakamoto [r,6], K. Nakamura [r,6], S. Nakayama [aw], T. Nakaya [ab], D. Naples [al], M.L. Navin [ar], B. Nelson [ah], T.C. Nicholls [au], C. Nielsen [e], K. Nishikawa [r,6], H. Nishino [ax], K. Nitta [ab], T. Nobuhara [ab], J.A. Nowak [ae], Y. Obayashi [aw], T. Ogitsu [r,6], H. Ohhata [r,6], T. Okamura [r,6], K. Okumura [ax], T. Okusawa [ai], S.M. Oser [e], M. Otani [ab,*], R.A. Owen [am], Y. Oyama [r,6], T. Ozaki [ai], M.Y. Pac [l], V. Palladino [w],

V. Paolone [al], P. Paul [ah], D. Payne [ad], G.F. Pearce [au], J.D. Perkin [ar], V. Pettinacci [o], F. Pierre [2], E. Poplawska [am], B. Popov [ak,5], M. Posiadala [bb], J.-M. Poutissou [az], R. Poutissou [az], P. Przewlocki [b], W. Qian [au], J.L. Raaf [d], E. Radicioni [v], P.N. Ratoff [ac], T.M. Raufer [au], M. Ravonel [p], M. Raymond [u], F. Retiere [az], A. Robert [ak], P.A. Rodrigues [1], E. Rondio [b], J.M. Roney [ba], B. Rossi [c], S. Roth [ap], A. Rubbia [o], D. Ruterbories [k], S. Sabouri [e], R. Sacco [am], K. Sakashita [r,6], F. Sánchez [s], A. Sarrat [h], K. Sasaki [r,6], K. Scholberg [m], J. Schwehr [k], M. Scott [u], D.I. Scully [bd], Y. Seiya [ai], T. Sekiguchi [r,6], H. Sekiya [aw], M. Shibata [r,6], Y. Shimizu [ax], M. Shiozawa [aw], S. Short [u], M. Siyad [au], R.J. Smith [aj], M. Smy [g], J.T. Sobczyk [bg], H. Sobel [g], M. Sorel [t], A. Stahl [ap], P. Stamoulis [t], J. Steinmann [ap], B. Still [am], J. Stone [d], M. Stodulski [q], C. Strabel [o], R. Sulej [b], A. Suzuki [aa], K. Suzuki [ab], S. Suzuki [r,6], S.Y. Suzuki [r,6], Y. Suzuki [r,6], Y. Suzuki [aw], J. Swierblewski [q], T. Szeglowski [as], M. Szeptycka [b], R. Tacik [an,az], M. Tada [r,6], M. Taguchi [ab], S. Takahashi [ab], A. Takeda [aw], Y. Takenaga [aw], Y. Takeuchi [aa], K. Tanaka [r,6], H.A. Tanaka [e,6], M. Tanaka [r,6], M.M. Tanaka [r,6], N. Tanimoto [ax], K. Tashiro [ai], I. Taylor [ah], A. Terashima [r,6], D. Terhorst [ap], R. Terri [am], L.F. Thompson [ar], A. Thorley [ad], W. Toki [k], S. Tobayama [e], T. Tomaru [r,6], Y. Totsuka [2], C. Touramanis [ad], T. Tsukamoto [r,6], M. Tzanov [ae,j], Y. Uchida [u], K. Ueno [aw], A. Vacheret [u], M. Vagins [g], G. Vasseur [h], T. Wachala [q], J.J. Walding [u], A.V. Waldron [aj], C.W. Walter [m], P.J. Wanderer [f], J. Wang [av], M.A. Ward [ar], G.P. Ward [ar], D. Wark [au,u], M.O. Wascko [u], A. Weber [aj,au], R. Wendell [m], N. West [aj], L.H. Whitehead [bd], G. Wikström [p], R.J. Wilkes [be], M.J. Wilking [az], Z. Williamson [aj], J.R. Wilson [am], R.J. Wilson [k], T. Wongjirad [m], S. Yamada [aw], Y. Yamada [r,6], A. Yamamoto [r,6], K. Yamamoto [ai], Y. Yamanoi [r,6], H. Yamaoka [r,6], T. Yamauchi [ab], C. Yanagisawa [ah,6], T. Yano [aa], S. Yen [az], N. Yershov [z], M. Yokoyama [av], T. Yuan [j], A. Zalewska [q], J. Zalipska [e], L. Zambelli [ak], K. Zaremba [bc], M. Ziembicki [bc], E.D. Zimmerman [j], M. Zito [h], J. Zmuda [bg]

[a] University of Alberta, Centre for Particle Physics, Department of Physics, Edmonton, Alberta, Canada
[b] National Center for Nuclear Research, Warsaw, Poland
[c] University of Bern, Albert Einstein Center for Fundamental Physics, Laboratory for High Energy Physics (LHEP), Bern, Switzerland
[d] Boston University, Department of Physics, Boston, MA, USA
[e] University of British Columbia, Department of Physics and Astronomy, Vancouver, British Columbia, Canada
[f] Brookhaven National Laboratory, Physics Department, Upton, NY, USA
[g] University of California, Irvine, Department of Physics and Astronomy, Irvine, CA, USA
[h] IRFU, CEA Saclay, Gif-sur-Yvette, France
[i] Chonnam National University, Institute for Universe & Elementary Particles, Gwangju, Republic of Korea
[j] University of Colorado at Boulder, Department of Physics, Boulder, CO, USA
[k] Colorado State University, Department of Physics, Fort Collins, CO, USA
[l] Dongshin University, Department of Physics, Naju, Republic of Korea
[m] Duke University, Department of Physics, Durham, NC, USA
[n] Ecole Polytechnique, IN2P3-CNRS, Laboratoire Leprince-Ringuet, Palaiseau, France
[o] ETH Zurich, Institute for Particle Physics, Zurich, Switzerland
[p] University of Geneva, Section de Physique, DPNC, Geneva, Switzerland
[q] H. Niewodniczanski Institute of Nuclear Physics PAN, Cracow, Poland
[r] High Energy Accelerator Research Organization (KEK), Tsukuba, Ibaraki, Japan
[s] Institut de Fisica d'Altes Energies (IFAE), Bellaterra (Barcelona), Spain
[t] IFIC (CSIC & University of Valencia), Valencia, Spain
[u] Imperial College London, Department of Physics, London, United Kingdom
[v] INFN Sezione di Bari and Università e Politecnico di Bari, Dipartimento Interuniversitario di Fisica, Bari, Italy
[w] INFN Sezione di Napoli and Università di Napoli, Dipartimento di Fisica, Napoli, Italy
[x] INFN Sezione di Padova and Università di Padova, Dipartimento di Fisica, Padova, Italy
[y] INFN Sezione di Roma and Università di Roma "La Sapienza", Roma, Italy
[z] Institute for Nuclear Research of the Russian Academy of Sciences, Moscow, Russia
[aa] Kobe University, Kobe, Japan
[ab] Kyoto University, Department of Physics, Kyoto, Japan
[ac] Lancaster University, Physics Department, Lancaster, United Kingdom
[ad] University of Liverpool, Department of Physics, Liverpool, United Kingdom
[ae] Louisiana State University, Department of Physics and Astronomy, Baton Rouge, LA, USA
[af] Université de Lyon, Université Claude Bernard Lyon 1, IPN Lyon (IN2P3), Villeurbanne, France
[ag] Miyagi University of Education, Department of Physics, Sendai, Japan
[ah] State University of New York at Stony Brook, Department of Physics and Astronomy, Stony Brook, NY, USA
[ai] Osaka City University, Department of Physics, Osaka, Japan
[aj] Oxford University, Department of Physics, Oxford, United Kingdom
[ak] UPMC, Université Paris Diderot, CNRS/IN2P3, Laboratoire de Physique Nucléaire et de Hautes Energies (LPNHE), Paris, France
[al] University of Pittsburgh, Department of Physics and Astronomy, Pittsburgh, PA, USA
[am] Queen Mary, University of London, School of Physics and Astronomy, London, United Kingdom
[an] University of Regina, Physics Department, Regina, Saskatchewan, Canada
[ao] University of Rochester, Department of Physics and Astronomy, Rochester, NY, USA
[ap] RWTH Aachen University, III. Physikalisches Institut, Aachen, Germany
[aq] Seoul National University, Department of Physics and Astronomy, Seoul, Republic of Korea
[ar] University of Sheffield, Department of Physics and Astronomy, Sheffield, United Kingdom
[as] University of Silesia, Institute of Physics, Katowice, Poland
[at] STFC, Daresbury Laboratory, Warrington, United Kingdom
[au] STFC, Rutherford Appleton Laboratory, Harwell Oxford, United Kingdom
[av] University of Tokyo, Department of Physics, Tokyo, Japan
[aw] University of Tokyo, Institute for Cosmic Ray Research, Kamioka Observatory, Kamioka, Japan

[ax] *University of Tokyo, Institute for Cosmic Ray Research, Research Center for Cosmic Neutrinos, Kashiwa, Japan*
[ay] *University of Toronto, Department of Physics, Toronto, Ontario, Canada*
[az] *TRIUMF, Vancouver, British Columbia, Canada*
[ba] *University of Victoria, Department of Physics and Astronomy, Victoria, British Columbia, Canada*
[bb] *University of Warsaw, Faculty of Physics, Warsaw, Poland*
[bc] *Warsaw University of Technology, Institute of Radioelectronics, Warsaw, Poland*
[bd] *University of Warwick, Department of Physics, Coventry, United Kingdom*
[be] *University of Washington, Department of Physics, Seattle, WA, USA*
[bf] *University of Winnipeg, Department of Physics, Winnipeg, Manitoba, Canada*
[bg] *Wroclaw University, Faculty of Physics and Astronomy, Wroclaw, Poland*
[bh] *York University, Department of Physics and Astronomy, Toronto, Ontario, Canada*

The T2K Collaboration

A R T I C L E   I N F O

A B S T R A C T

Precise measurement of neutrino beam direction and intensity was achieved based on a new concept with modularized neutrino detectors. INGRID (Interactive Neutrino GRID) is an on-axis near detector for the T2K long baseline neutrino oscillation experiment. INGRID consists of 16 identical modules arranged in horizontal and vertical arrays around the beam center. The module has a sandwich structure of iron target plates and scintillator trackers. INGRID directly monitors the muon neutrino beam profile center and intensity using the number of observed neutrino events in each module. The neutrino beam direction is measured with accuracy better than 0.4 mrad from the measured profile center. The normalized event rate is measured with 4% precision.

1. Introduction

To investigate neutrino flavor mixing [1,2] and mass splittings, long baseline (over 100 km) neutrino oscillation experiments are currently running and also being prepared. In these experiments, it is extremely important to measure the beam direction and intensity to ensure the stable neutrino production from a primary proton beam.

T2K (Tokai-to-Kamioka) [3] is a long baseline neutrino oscillation experiment. An intense muon neutrino beam is produced by using the 30-GeV proton synchrotron at J-PARC (Japan Proton Accelerator Research Complex) in Tokai. The proton beam strikes a graphite target to produce charged pions, which are focused by three magnetic horns. The pions decay mainly into muon–muon–neutrino pairs during their passage through the 96-m decay volume. After traveling 295 km, the neutrinos are detected by the Super-Kamiokande (SK) detector [4] in the Kamioka Observatory (Fig. 1). The goals of the T2K experiment are to measure oscillation parameters with a precision of $\delta(\sin^2 2\theta_{23}) \sim 0.01$ and $\delta(\Delta m^2_{23}) \sim 10^{-4} \text{ eV}^2$ via ν_μ disappearance and to investigate θ_{13} through $\nu_\mu \rightarrow \nu_e$ oscillation.

T2K adopts an off-axis beam configuration [5]; the beam center direction is $2.5°$ away from the direction of SK so that the muon neutrino beam has a narrow energy peak at ~ 0.6 GeV, which maximizes the effect of the neutrino oscillation at SK and minimizes the background for the signal. The neutrino energy varies as a function of the off-axis angle. Therefore, it is important to monitor

and control the beam direction precisely; the beam direction is required to be controlled within ± 1 mrad. In addition, monitoring of the beam intensity is important to ensure stable neutrino beam production. A muon monitor [6] located downstream of the beam dump measures the beam direction and stability by detecting muons from decay of the secondary mesons for every bunch. Since the muon monitor detects only high energy muons which penetrate the beam dump, the momentum and the exit angle (phase space) of the parent mesons covered by the muon monitor is different to the one of pions which produce neutrinos to the near or far detectors. INGRID is an on-axis near detector and measures the neutrino beam direction and intensity by detecting neutrino interaction events. The covered phase space of the parent mesons are much closer to the one for the off-axis neutrino detectors than the muon monitor. Therefore, the measurement by INGRID is more directly connected with the neutrino energy spectrum and the neutrino flux. It was designed to provide daily measurements of the beam direction with a sufficient statistics at the design beam intensity (750 kW primary proton beam power).

This paper reports neutrino beam measurements using the INGRID detector based on the first two physics runs: Run I (January–June 2010) and Run II (November 2010–March 2011). The range of the beam intensities is from 8 kW to 145 kW. During this time period, INGRID recorded more than 99.6% of delivered beam corresponding to 1.44×10^{20} protons on target (POT). The reasons of missing 0.4% POT are the dead time during switching of
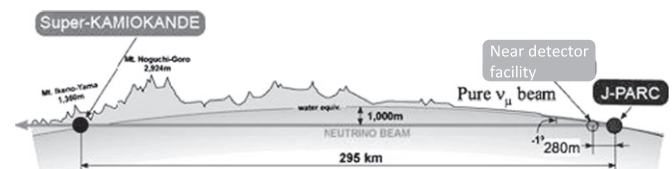

Fig. 1. Schematic view of the T2K experiment configuration. The near detector facility houses an off-axis detector and the on-axis INGRID detector.

a INGRID data acquisition (DAQ) run, trouble of the INGRID DAQ system and so on. Using data from the same period, the T2K experiment observed indications of $\nu_\mu \to \nu_e$ appearance [7].

In Sections 2 and 3, the design and basic performance of the INGRID detector are described, respectively. Details of Monte Carlo (MC) simulations and criteria for neutrino event selection are described in Sections 4 and 5, respectively. In Section 6, results of neutrino beam measurements with INGRID are summarized.

2. Detector configuration

INGRID is located 280 m downstream of the meson production target, where the spatial width (1σ) of the neutrino beam is about 5 m. Therefore, it is designed to sample the beam in a transverse section of $10\,m \times 10\,m$ with 14 identical modules arranged as two identical groups along the horizontal and vertical axes. Two separate modules are placed at off-axis positions off the main cross, as shown in Fig. 2 to monitor the asymmetry of the beam.

Each of the modules consists of a sandwich structure of 9 iron target plates and 11 tracking scintillator planes as shown in Fig. 3. They are surrounded by veto scintillator planes (Fig. 3, right) to reject charged particles coming from outside the modules. The dimensions of the iron target plates are $124 \times 124\,cm^2$ in the horizontal and vertical directions and 6.5 cm along the beam
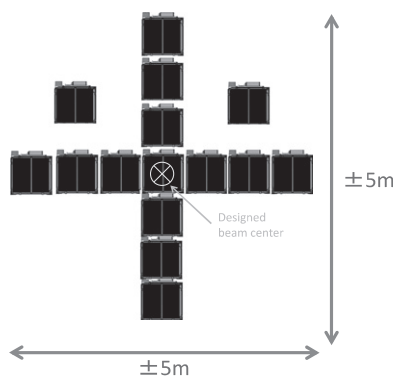
Fig. 2. The 16 identical modules sample the neutrino beam in a transverse section of $10\,m \times 10\,m$. The vertical row locates upstream of the horizontal row. The center of the cross, where the center module of the vertical row and that of the horizontal row are installed along the beam direction, corresponds to the designed neutrino beam center ($\theta = 0°$).

direction. The total iron mass serving as a neutrino interaction target is 7.1 t per module. Neutrino interaction events are selected by reconstructing the track of charged particles generated by interactions in the iron target. The horizontal and vertical profiles are reconstructed from the number of observed events in each module. The beam center is measured from the center of the horizontal and vertical profiles. Each of the 11 tracking planes consists of 24 scintillator bars in the horizontal direction optically isolated glued with CEMEDINE® PM200 to 24 perpendicular bars in the vertical direction. Each of the veto planes consists of 22 scintillator bars segmented along the beam direction. There are 9592 scintillator bars in total. Iron plates were not placed between the 10th and 11th tracking planes.

All the INGRID scintillator bars were produced at Fermilab [8]. The scintillator bars are made of polystyrene, infused with PPO (1%) and POPOP (0.03%), and are produced by extrusion in the shape of a rectangular cross-section ($1.0\,cm \times 5.0\,cm$). A white reflective coating composed of TiO_2 infused in polystyrene is co-extruded. One end of the rectangular face, far from the photo-detector, is painted with ELJEN® EJ-510. The length of the scintillator bars is 120.3 cm, 111.9 cm and 129.9 cm for tracking, top/bottom veto and right/left veto planes, respectively. A hole whose diameter is about 3 mm at the center of the scintillator bar allows the insertion of a wavelength shifting (WLS) fiber for light collection.

The WLS fiber, Y11(200)M by Kuraray [9] is used for the light collection. The diameter of the fibers is 1.0 mm and fits the active region of the photo-detector ($1.3 \times 1.3\,mm^2$). The fibers are cut to the lengths of the scintillators and the cut surfaces are polished with diamond blades (Fiberfin Inc. FiberFin 4). One side of the fiber is attached to a Multi Pixel Photon Counter (MPPC, Hamamatsu S10362-13-050C) [10,11] with a specially developed connector [12]. The other side is painted with ELJEN® EJ-510 to increase the light yield at the far side.

The MPPC signal is transported to the front-end electronics by a co-axial cable (Hirose U.FL-2LP-068). The front-end electronics is contained in a aluminum box attached to the top-right side of the scintillator plane. The integrated charge and hit timing are digitized and recorded with a 2.5 photo-electron (PE) threshold. The bias voltage applied to the MPPCs is 70 V typically and controlled by the front-end electronics with a precision of 0.02 V whereas the requirement is less than 0.1 V. The voltage change of 0.02 V corresponds to the MPPC gain change of 2% and this makes negligibly small effect on the neutrino event selection. A detailed description of the electronics can be found in Ref. [13].

Fig. 4 shows an example of a neutrino event candidates in one of the modules.
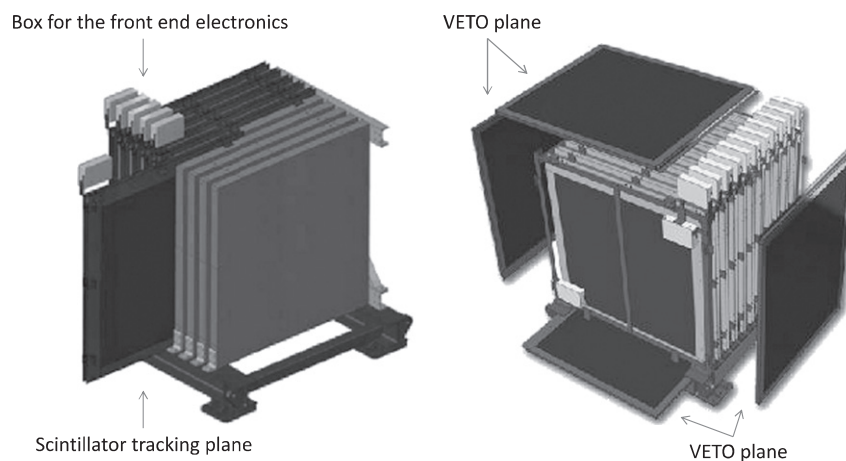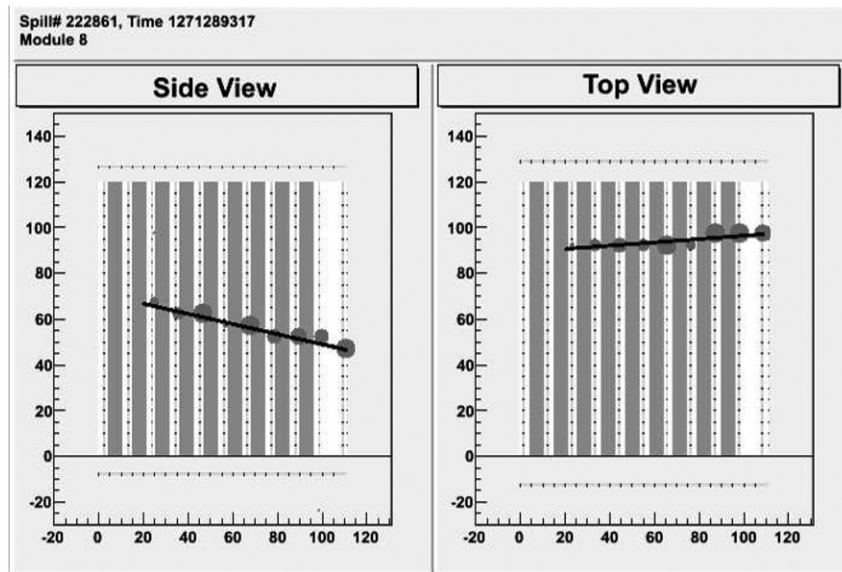

Fig. 3. Structure of the module which is a sandwich made of 9 iron target plates and 11 scintillator trackers (left). The module is surrounded by the scintillator veto planes (right). Each scintillator tracking plane has a front-end electronics board, which is contained inside an aluminum box attached to the top-right side of the plane.

Fig. 4. Typical neutrino interaction event candidate in one of the modules. A beam neutrino enters from the left. The size of the circles is proportional to the observed number of PE at scintillator bars, and black lines show the reconstructed tracks.
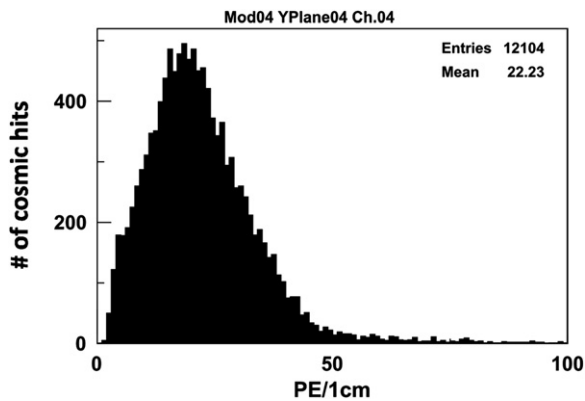

Fig. 5. Typical yields distribution. Light yield is normalized by the path length.
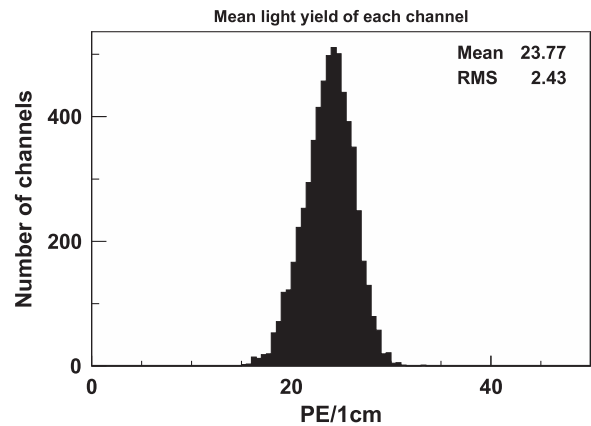

Fig. 6. Mean light yields.

3. Basic performance of the detector

INGRID identifies neutrino events by detecting tracks from muons. The hit efficiency for muon tracks is monitored with the beam induced muons (described in Section 5.3) incoming from outside of the detector. The mean light yield and timing resolution are monitored with cosmic-ray data.

3.1. Mean light yield

The mean light yield per 1 cm of a muon track is monitored with inter-spill cosmic-ray data for each scintillator bar. A typical light yield distribution of one channel is shown in Fig. 5. The distribution is consistent with the Landau distribution. The mean light yields of all the channels are shown in Fig. 6. The average mean light yield normalized to unit length is 24 PE/cm.

3.2. Hit efficiency

The hit efficiency is evaluated by muons with the following procedure; the muon track is reconstructed without using the hit information in the scintillator plane being evaluated, and then in that plane, channels expected to have hits from the track trajectory are checked whether they have a hit or not. The beam induced muons pass almost straight along the beam direction. The cosmic-ray muons pass at least seven planes due to the trigger algorithm and the angular distribution is different among the scintillator bars. Therefore, the beam induced muon is used for the comparison of the channel by channel hit efficiency. On the other hand, the cosmic-ray muons are used to measure the hit efficiency as a function of the track angle.

Fig. 7 shows the result of the hit efficiency measurement with the beam induced muons. Fig. 8 shows the efficiency as a function of the track angle measured using cosmic-ray muons. The track angle is defined as the angle between the designed beam direction and the reconstructed track. The main reason for the inefficiency is because of the small gap between scintillator bars, so the efficiency depends on track angle; a particle with small angle has more probability to go through the gap. As a result, the efficiency is smaller than that expected from PE statistics with measured light yield described in Section 3.1. The measured inefficiency is consistent with the expectation from the actual gap size. The gap size in the MC simulation is tuned finely based on the actual gap size and the efficiency is consistent between the data and the MC simulation within 1%.
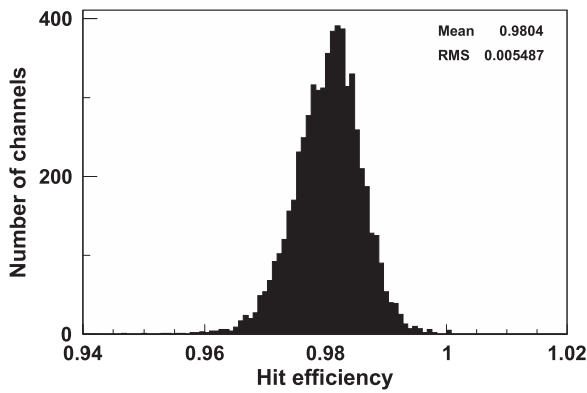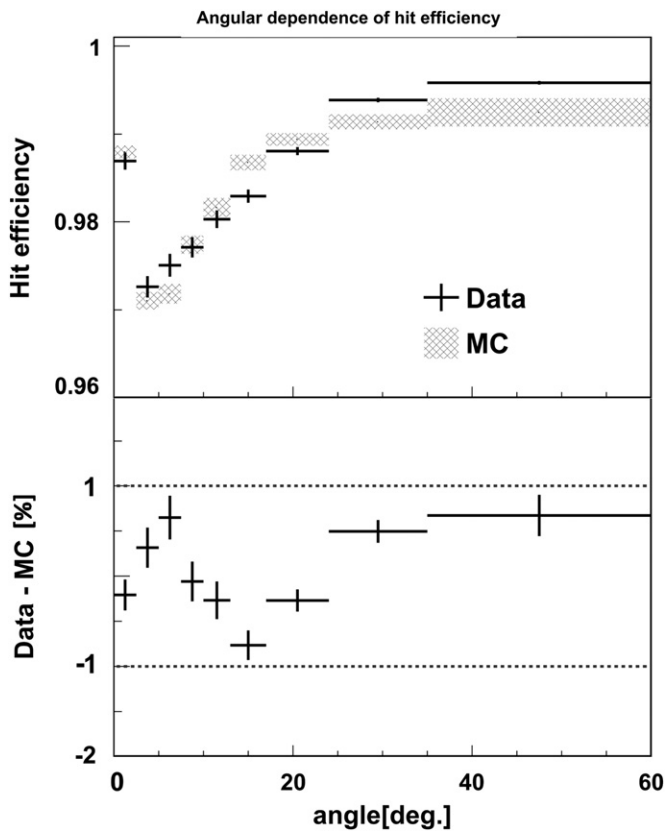
Fig. 7. Hit efficiency for all channels.

Fig. 8. Hit efficiency as a function of reconstructed track angle measured by cosmic-ray data.
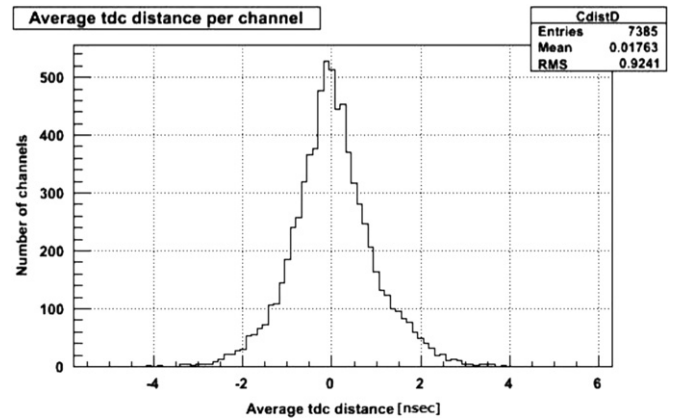

Fig. 9. Time difference of hit channels from the average hit times for cosmic-ray tracks.
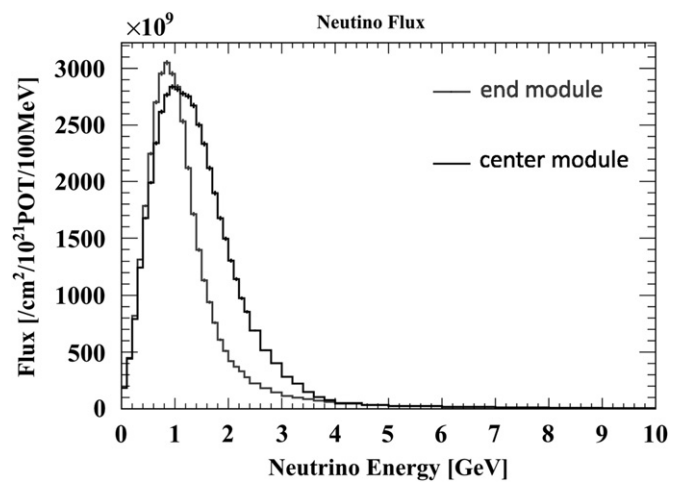
Fig. 10. Neutrino energy spectrum predicted by JNUBEAM at the center and end modules.

3.3. Hit timing resolution

Hit timing resolution is estimated by measuring the time difference among hit channels for cosmic-ray tracks. Fig. 9 shows the time differences of each hit channel from the average of all channels after the correction for differences in the readout cable length and the light propagation time through the fiber. The RMS is 0.9 ns, which corresponds to the timing resolution if all the channels have the same resolution. The width of the primary proton beam bunch was about 30 ns during RUNS 1 and 2, so this resolution is sufficient for selecting the beam events.

4. Monte Carlo simulations for the neutrino beam measurements

The Monte Carlo (MC) simulations for the neutrino beam measurements consist of three main parts. The first is a simulation

of the neutrino beam production, which predicts the neutrino flux and energy spectrum of each neutrino flavor. The second is a neutrino interaction simulation, which calculates the cross-section of the neutrino interaction and kinematics of final state particles taking into account the intranuclear interactions of hadrons. The third step is a detector response simulation to reproduce the scintillator light yield, and the response of WLS fibers and MPPC.

4.1. Neutrino beam prediction

To predict neutrino fluxes and energy spectra, a neutrino beam Monte Carlo simulation, called JNUBEAM [3], was developed based on the GEANT3 framework [14]. We compute the neutrino beam fluxes starting from models (FLUKA [15,16] and GCALOR [17]) and tuning them to experimental data (NA61/SHINE [18] and Ref. [19]). Energy spectra at the center and end horizontal modules are shown in Fig. 10. Because each module covers a different off-axis angle, the neutrino energy spectrum at each module location is different. The difference in the average neutrino energy between the center module and the end module is about 0.2 GeV. The energy spectrum is generated at each module to estimate the MC expectation. Energy spectra at 10 m upstream from INGRID are predicted with the same procedure in order to simulate the background events from neutrino interactions in the wall of the experimental hall.

4.2. Neutrino interaction simulation

Neutrino interactions with iron and scintillator in INGRID are simulated using the NEUT program libraries [20]. Combined with the neutrino flux predicted by JNUBEAM, we expect about 4×10^7 neutrino interactions for 10^{21} POT in the 14 modules consisting of horizontal and vertical rows. For the background event simulation, the neutrino interactions on an equal mix of carbon and hydrogen are generated uniformly in the 5 m deep slice of the upstream wall. The decay volume end is about 150 m upstream from the start of the slice. The earth upstream of the wall is mainly sand, but for simplicity carbon and hydrogen are used in the simulation. The number of generated interactions is normalized by the beam induced muon events (described in Section 5.1.5) in data.

4.3. INGRID detector response simulation

Detector response simulation was developed with the Geant4 framework [14]. The simulation includes a detailed geometry of the experimental hall.

The energy deposit in each scintillator bar is simulated by Geant4 library and is converted to the number of PE at each MPPC. The conversion factor from the energy deposit to a number of PE is determined based on the measured light yields with cosmic-rays. The cross-section of the scintillator bar is tuned to reproduce the hit inefficiency due to the dead region of the bar. The scintillator quenching effect is simulated using Birk's law
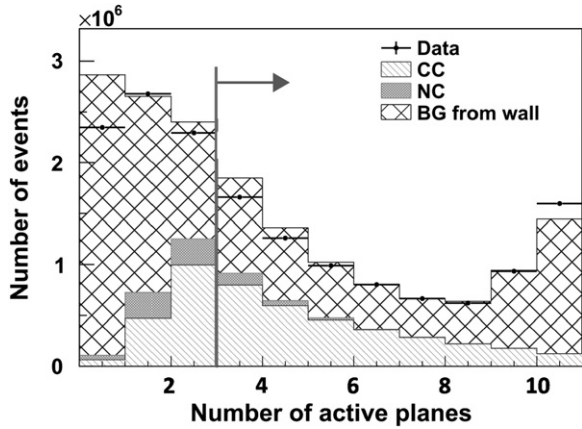
with the value measured in Ref. [21]. Attenuation in the fiber is taken into account based on the measured attenuation length [22]. The response of MPPC, such as saturation due to the finite number of photo-diodes, is modeled based on test bench measurements [23].

The dimensions and mass of the iron target plates are implemented with the design value. For analysis, we make a correction for the measured mass difference for each iron plate, as described in Section 5.3.

5. Neutrino event selection

The neutrino beam profile is reconstructed from the number of neutrino interaction events at each module. This section describes the selection procedure for neutrino interactions and the systematic error.

5.1. Selection criteria

A neutrino interaction event is identified by a long track from a charged particle generated by the neutrino interaction. First, pre-selections are applied to reject accidental noise events. Then, tracks are reconstructed using hit information. After that, charged particles from outside of the module are rejected with the veto planes and the reconstructed event vertex is required to be inside the fiducial volume (FV). In these selections, each module is treated separately. The event selection criteria are described in the following sections.

5.1.1. Event definition
When there are four or more hits in a 100 ns time window, all hits within this time window compose an event. The 100 ns time window is sufficiently large compared to the beam width of 30 ns and the hit timing resolution of 0.9 ns (Section 3.3).

5.1.2. Pre-selections
A tracking plane with at least one hit in both x and y layers is defined as an "active" plane. We use a right hand coordinate in which z is along the beam direction and y is upward in the vertical direction. Events with three or more active planes are selected as shown in Fig. 11. There is a discrepancy in the number of events with no active plane between data and MC. Fig. 12 shows a MC event display of a typical event with no active plane. The first tracking plane is not counted as an active plane, but are used for veto. Most of the events originate in low energy particles produced by the neutrino interaction upstream of the wall of
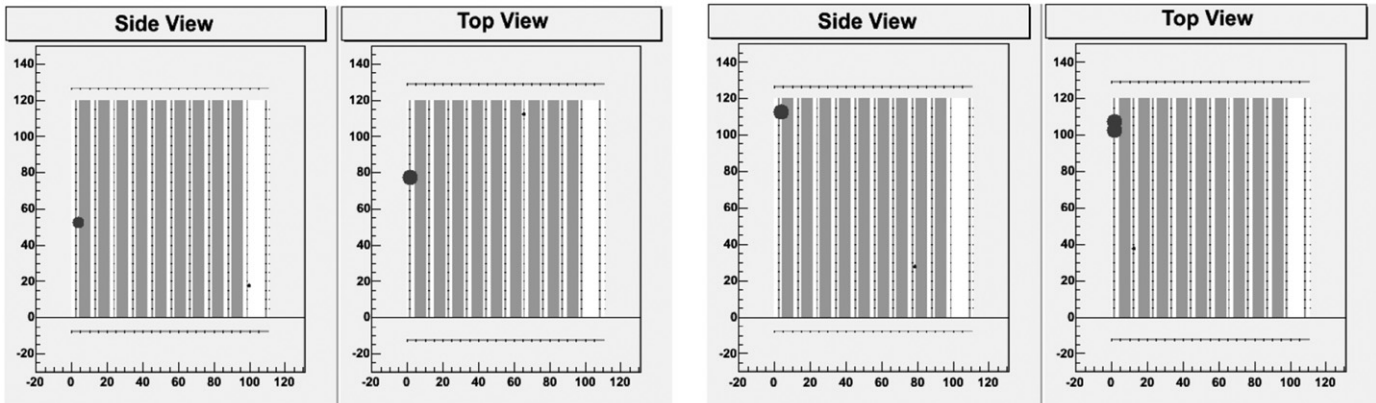

Fig. 11. Number of active planes. Events with more than two active planes are selected.

Fig. 12. Examples of the MC event with no active plane. The circle in the left most plane shows a hit by the particle and other circle shows a hit by MPPC noise.

the experimental hall. We consider that the discrepancy is caused by uncertainties in the simulation of these low energy particles.

After the selection with the number of active planes, light yields averaged over x or y layers of the active planes are required to be larger than 6.5 PE for both x layers and y layers as shown in Fig. 13; inefficiency due to this selection is negligible for muon tracks.

5.1.3. Tracking

After pre-selection, tracks in x–z and y–z projections are reconstructed independently with a simple algorithm; first, hits in the most downstream active layer are adopted as the end point of the track. Then the track is extrapolated to upstream layers by checking the upstream hits. A hit is included in the track if the hit position is within two scintillator bars from the straight line extrapolated from the downstream hits. Fig. 14 shows an example of a reconstructed track. Tracking efficiency is checked with cosmic-ray data and the efficiency is $\sim 95\%$ for cosmic-rays passing three scintillator planes.

The vertex position is reconstructed as the most upstream point of the track for each projection. The track angle is obtained by fitting the hits composing the track with a straight line. Figs. 15 and 16 show differences between true and reconstructed x and z vertices, respectively, for MC events. The RMS for the x vertices is 2.7 cm. Fig. 17 shows the distribution of 3D angle between true and reconstructed muon tracks for MC events. The RMS is 3.8°.

After the tracking, some badly fitted tracks are rejected by using the position difference of the vertex z between x–z and y–z projections. The difference is required to be within ± 1 plane, as shown in Fig. 18.

5.1.4. Timing cut

To reject off-timing events such as cosmic-ray events, only events of ± 100 ns from the expected timing are selected (Fig. 19). The expected timing is evaluated with the primary proton beam
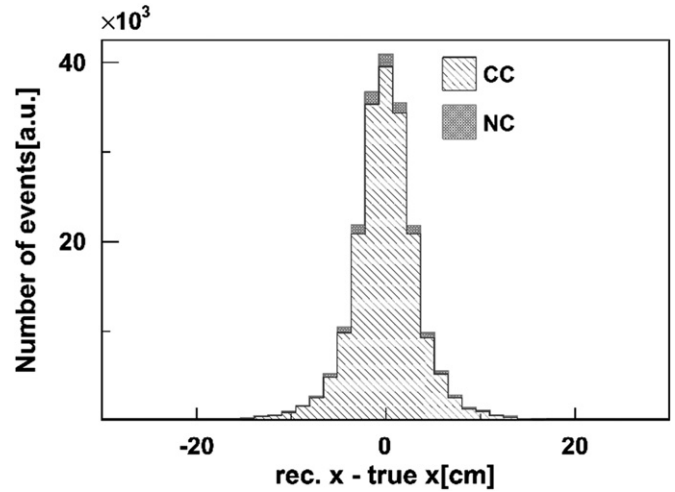

Fig. 15. Differences between true and reconstructed vertex position in the x direction for MC events.
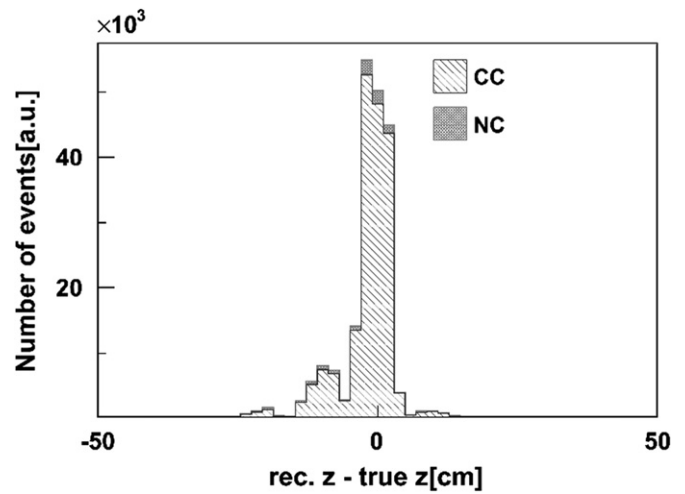

Fig. 16. Differences between true and reconstructed vertex position in the z direction for MC events.

Fig. 13. Light yield averaged over active layers. Events with more than 6.5 PE are selected.
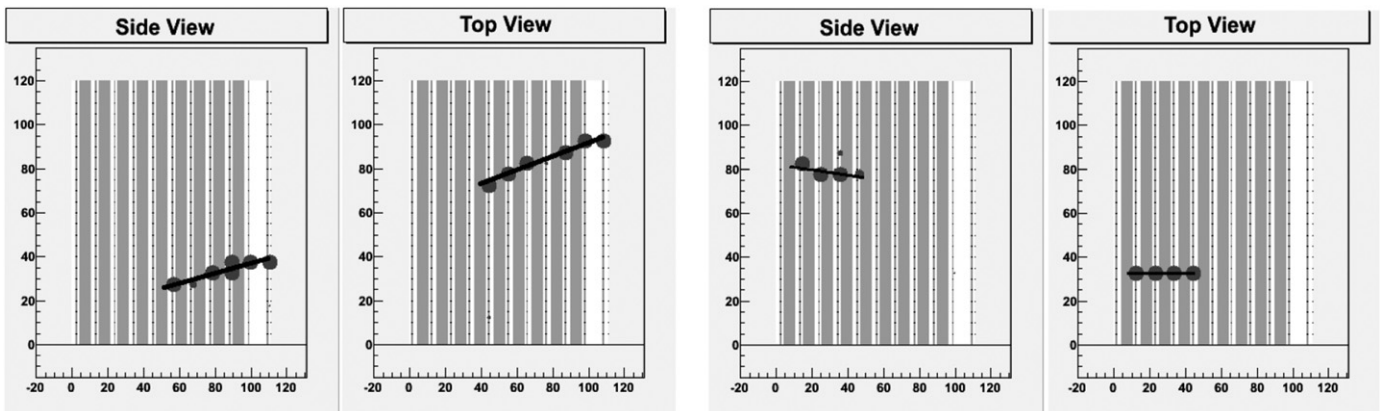

Fig. 14. Examples of the reconstructed tracks. The size of the circles shows the observed number of PE at scintillator bars, and black lines show the reconstructed tracks.
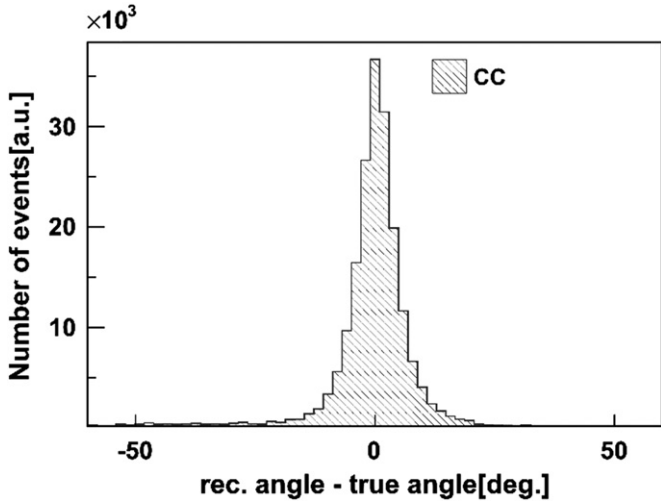
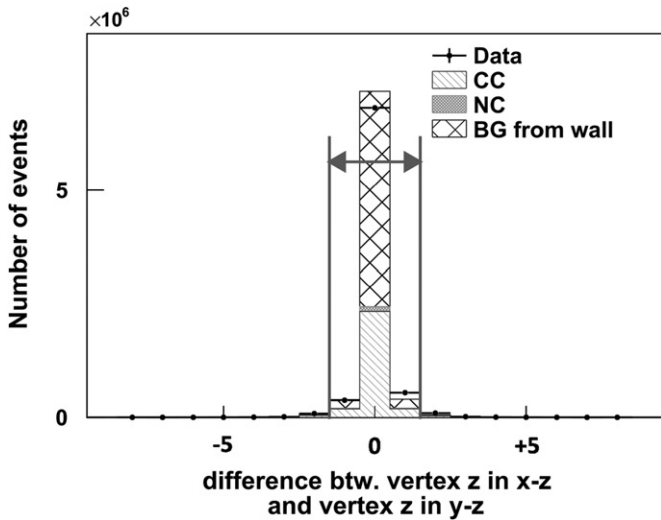**Fig. 17.** Angles between true and reconstructed tracks.

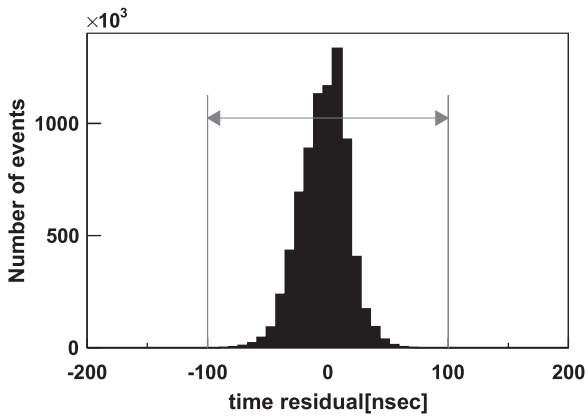**Fig. 18.** Difference of the z vertex position between x–z and y–z projections.

Fig. 19. Time difference between measured event timing and expected neutrino event timing. Events within ± 100 ns are selected.

timing [3], the time of flight of the particles from the target to INGRID, and the delay of the electronics and cables. The event timing is defined by the timing of the vertex hit.

5.1.5. Veto and fiducial volume (FV) cuts

Two selections are applied to reject incoming particles produced by neutrino interactions in the upstream material, such as the wall of the experimental hall. First, events which have a hit in a veto plane or the first tracker plane at the upstream position extrapolated from the reconstructed track are rejected. Events rejected by the veto cut are shown in Fig. 20. After the veto cut, the fiducial volume (FV) cut is applied. The FV of each module is defined as a volume composed of the 3rd–22nd of the 24 scintillator bars in the x and y directions, and from the second to the ninth tracker plane in the z direction. Events having a vertex inside the FV are selected as shown in Fig. 21. The events rejected by these selections are identified as 'beam induced muon' events.

Fig. 22 shows the vertex distributions in the x and y directions after all cuts. The fraction of the background in the selected events is 0.4%. Note that the backgrounds seen in the FV in the x direction are rejected by the FC cut in the y direction.

5.1.6. Event selection summary

The result of the event selection is summarized in Table 1. The MC simulation includes neutrino interactions in the wall of the experimental hall. The number of neutrino interactions in the wall is normalized by the number of beam induced muons with # of active planes > 2 in the real data. The MC simulation reproduces the reduction in data well.

5.2. Selection efficiency

The neutrino event selection efficiency as a function of true neutrino energy is estimated by the MC simulation and is shown in Fig. 23. The efficiency averaged over the neutrino energy is different by about 4% between the modules. The $\sim 20\%$ inefficiency at high energy for the CC interaction is due to the events in which muons are produced with a rather large angle: for such events, the muon escapes from the module before it penetrates two iron plates.

5.3. Correction factors

In order to compare the data with the MC expectation, some corrections are applied to the number of selected neutrino events. The correction factors are for the iron target mass and accidental MPPC noise.

The neutrino interactions in the MC simulation are generated with the design mass of iron target plates, so a correction is applied to the neutrino interaction rate in each module individually based on the difference between the design mass and the measured one: $-1 \sim +1\%$ for each module.

Accidental MPPC noise hits sometimes results in mis-identification of the vertex. The dependence on the event selection as a function of MPPC noise rate is estimated by a MC simulation where the PE distribution and hit timing distribution are varied to reproduce data noise rates. According to this estimation and measured noise rate, the number of selected events is decreased by 3% with the existence of MPPC noise. The number of events in the MC simulation is corrected to account this effect.

5.4. Systematic errors

In this section the systematic error on the number of selected events is described. We describe both the errors related to the event selection criterion and the correction described in Section 5.3.
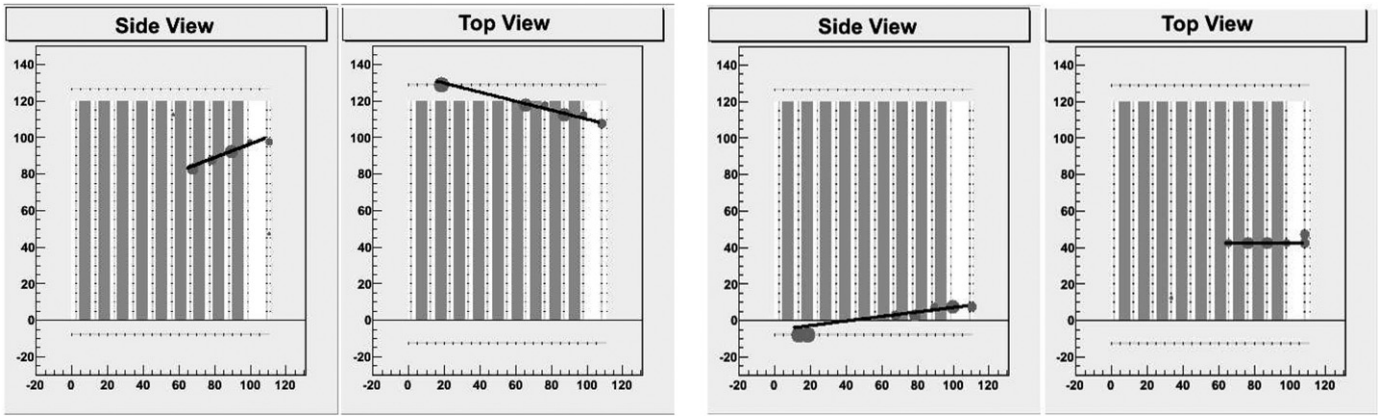
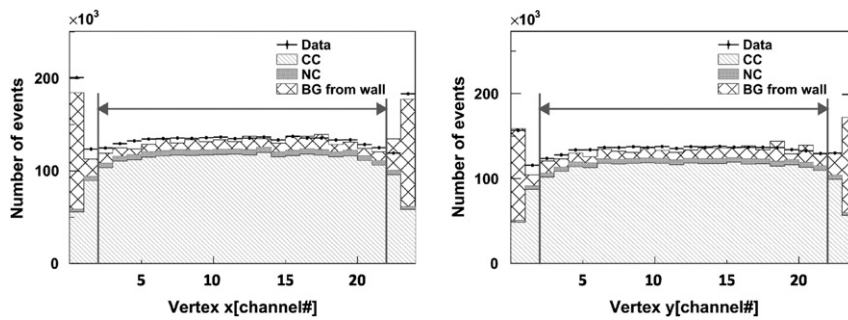**Fig. 20.** Event displays of rejected events by the veto cut.

Fig. 21. Vertex x and y distributions. A volume composed of the 3rd–22nd scintillator bars in the x and y directions is defined as fiducial volume (FV).
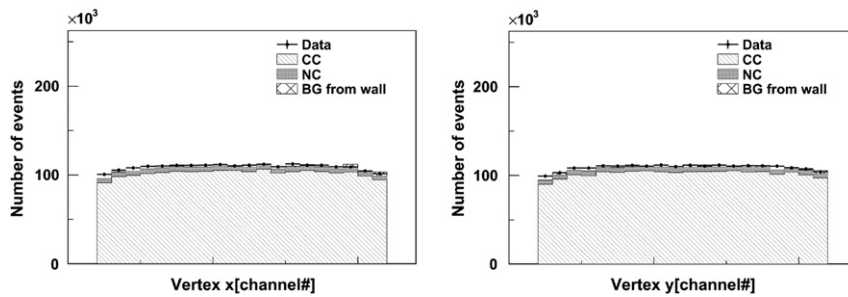

Fig. 22. Vertex x and y distributions after all the event selections.

Table 1

Event selection summary with all the 14 modules for 2.44×10^{20} POT. MC sample is normalized by POT. The MC simulation includes neutrino interactions in the wall of the experimental hall. The number of neutrino interactions in the wall is normalized by the number of the beam induced muons in the real data.

Selection	Data	(%)	MC	(%)
1 # of active planes >2	8.53×10^6	100	9.02×10^6	100
2 PE/active layers >6.5	8.53×10^6	99.9	9.02×10^6	99.9
3 Tracking	8.01×10^6	94	8.40×10^6	93
4 Track matching	7.74×10^6	91	8.10×10^6	90
5 Beam timing	7.73×10^6	91	8.10×10^6	90
6 Veto cut	3.30×10^6	39	3.30×10^6	37
7 FV cut	2.18×10^6	26	2.17×10^6	24

The systematic error of the light yield selection is negligible because the threshold value for the selection (6.5 PE/active layer) is much smaller than the measured light yield from cosmic-ray.
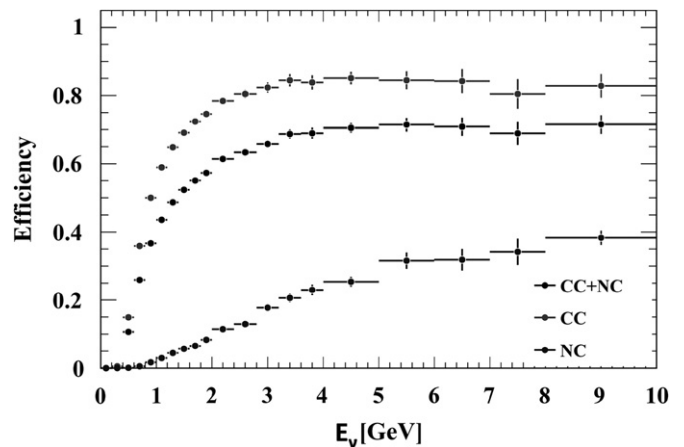
Fig. 23. Neutrino event selection efficiency as a function of true neutrino energy.

The systematic error of the tracking efficiency is estimated by comparing the efficiency for several lengths of track between the data and the MC simulation. The difference is larger for the shorter track events and the maximum difference of 1.4% is taken as the systematic error. For the selection on the difference of vertex z between x–z and y–z projections, the systematic error is estimated by looking at the change of the selection efficiency when varying the selection threshold. The difference (2.7%) between this and the nominal selection is taken as the systematic error. To estimate the systematic error associated with the FV selection, the number of neutrino events is re-counted as the fiducial volume is varied. In order to check the contamination of the beam induced muon from the edge, the fiducial volume is separated to center, middle and edge parts with the same volume. The difference of the event rate per unit volume is 1.1%, which is taken as the systematic error. The discrepancy between the hit efficiency measured with the beam induced muon event and that of the MC simulation is assigned as the uncertainty in the hit detection efficiency. The relation between the hit efficiency and the number of selected events is estimated by the MC simulation. A systematic error of 1.8% is assigned. The timing measurement is good enough that the systematic uncertainties resulting from the beam timing cut and out-of-beam events are negligible. There is a discrepancy between the beam induced muon event rate estimated by the MC simulation and that measured from the data. The change in the background contamination fraction from this discrepancy is estimated to be 0.2%, which is taken as the systematic error for the beam-related background correction.

The uncertainty of the iron mass measurement, 0.1%, is taken as the systematic error for the iron mass. The change in the selection efficiency due to the time variation of the measured noise rate is estimated to be 0.7%, which is taken as the systematic error for the MPPC noise correction.

Table 2 shows a summary of the systematic errors. The total systematic error is calculated as a quadratic sum of the errors and is 3.7%. In addition, there is 2% uncertainty for the normalization due to the systematic error on the POT measurement.

6. Results of the measurement

6.1. Event rate and comparison with the MC expectation

Figs. 24 and 25 show the daily rates of the neutrino events and the beam induced muon events normalized by protons on target (POT). The beam induced muon events are defined as the events rejected by the veto cut or the FV cut in Section 5. They are measured typically with statistical errors of 1.7% and 1.1% each day, respectively. The average event rate is slightly decreased (-0.9%) on February 4, 2011. This is considered to have been caused by a change in the primary beamline condition. The muon yield measured by the muon monitor showed a consistent tendency. The chi-squared values calculated from the average rates of the neutrino
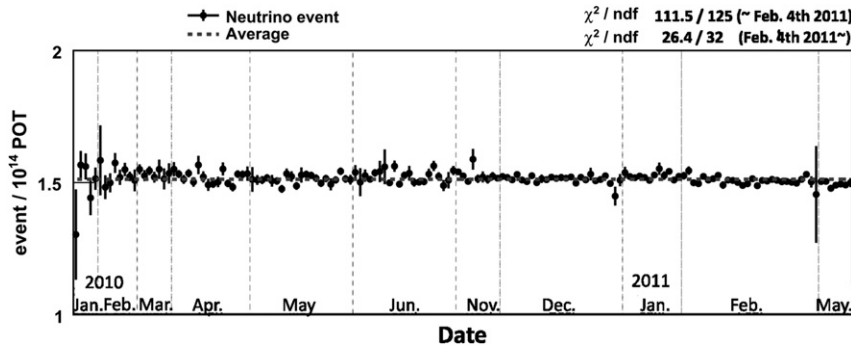
Table 2
Detector systematic errors.

Item	Error (%)
Average light yield per active layer	< 0.1
Tracking efficiency	1.4
Vertex z matching	2.7
FV cut	1.1
Hit efficiency	1.8
Out-of-beam events	< 0.1
Beam timing selection	< 0.1
Beam-related background events	0.2
Iron mass	0.1
Accidental MPPC noise	0.7
Total	3.7

Fig. 24. Daily event rate of the neutrino events normalized by protons on target.
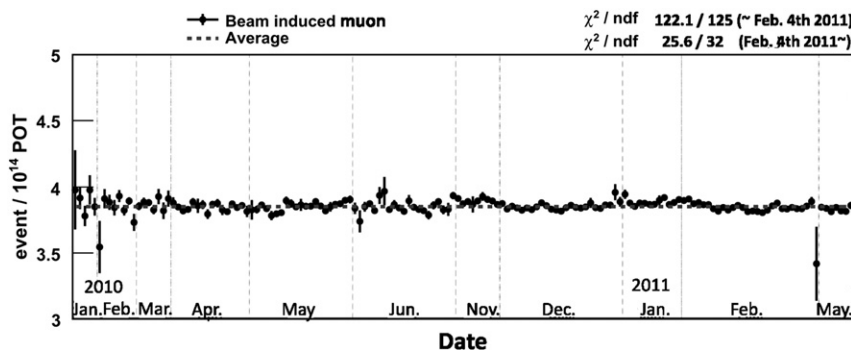

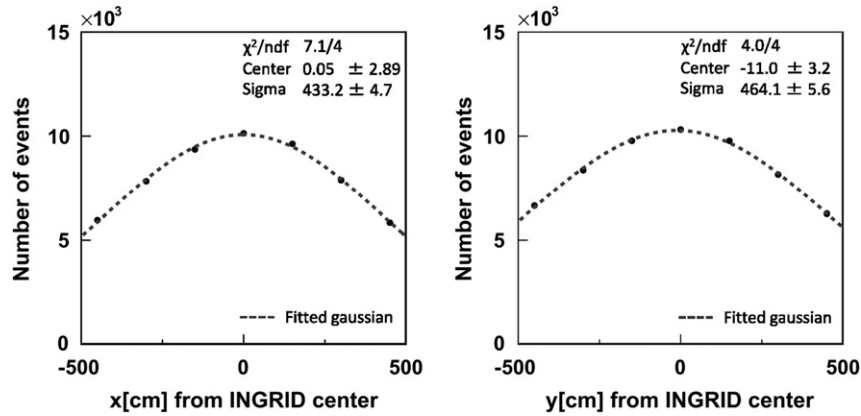**Fig. 25.** Daily event rate of the bean induced muon events normalized by protons on target.

Fig. 26. Neutrino beam profiles for x (left) and y (right) directions measured in April 2010. The error bars are the statistical errors and the error size is about 1%.

events (beam induced muon events) before and after February 4, 2011 are 111.5 (122.1) for 125 data points and 26.4 (25.6) for 32 data points, respectively. The event rate in INGRID before and after February 4, 2011 remained stable within statistical error and the beam intensity is stable during each of these two periods.

The data to MC ratio of the neutrino event rate is calculated to be 1.06 ± 0.001 (stat.) ± 0.04(detector syst.) ± 0.02(POT error). The uncertainties from the neutrino flux prediction and neutrino interaction model are not included in the systematic error.

6.2. Beam direction

The profile of the beam in the x and y directions is reconstructed with the number of neutrino events in seven horizontal and seven vertical modules, respectively. The observed profiles are fitted with a Gaussian function. The profile center is defined as the peak of the fit. Finally, the beam direction is reconstructed as the direction from the proton beam target position to the measured center at INGRID.

In order to monitor the stability of the beam direction with sufficient statistics at the current beam intensity, the number of neutrino events is accumulated on a monthly basis. Different accelerator run periods, for which the proton beam condition might be slightly different, are treated separately. Fig. 26 shows the observed profiles in April 2010. The error bars in Fig. 26 indicate the statistical error and the error size is about 1%. Black points in this figure show the number of neutrino events in each module and the dashed lines show the fitted Gaussian.

The points in Fig. 27 show the history of the beam centers in the x and y directions. All the points were stable well within 28 cm, which corresponds to the requirement of 1 mrad for the beam direction. Because beam direction was adjusted in November 2010, the beam centers in the y direction for later months are slightly shifted toward the center.

The systematic error of the profile center measurement was estimated by a toy MC simulation. In the simulation, the number of events at each module is changed within the range of the total detector systematic error of 3.7%. A total of 100,000 profiles are generated and RMSs of reconstructed center values are taken as the systematic errors; 9.2 cm and 10.4 cm for the x and y center, respectively.

From the beam center measurement and the survey between the proton target and the INGRID detectors, the average beam direction in x and y direction are measured as -0.014 ± 0.025(stat.)± 0.33 (syst.) mrad and -0.107 ± 0.025(stat.)± 0.37 (syst.) mrad, respectively. The beam direction is measured with a precision better than the requirement.
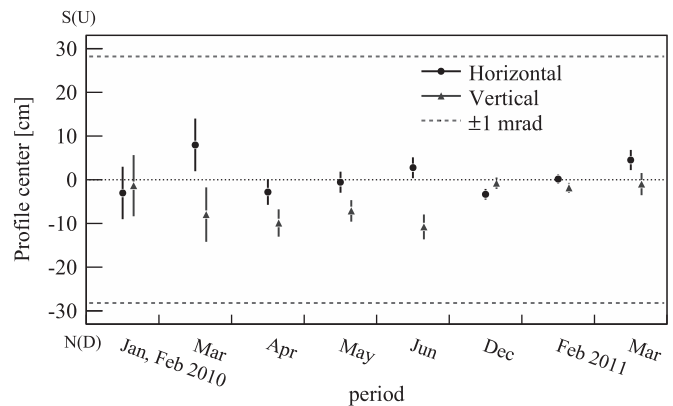

Fig. 27. History of the neutrino beam centers. The error bar shows the statistical errors on the mean.

7. Conclusion

We have reported the muon neutrino beam measurement with the T2K on-axis near neutrino detector, INGRID, for the T2K Run I and Run II data (1.44×10^{20} POT in total). INGRID consists of 14 identical modules arranged in a cross around the beam center. This configuration enables us to sample the beam in a sufficiently wide area to measure the beam center with a minimum of material.

The neutrino event rate is measured on a daily basis and remains stable within the statistical error, which is typically 1.7%. The data/MC ratio of the event rate is measured to be 1.06 ± 0.001(stat.)± 0.04(detector syst.)± 0.02(POT error).

Beam centers in the x and y directions are measured on a monthly basis and are stable well within 28 cm, which corresponds to the required 1 mrad in angle. The angle between the expected and measured beam center direction in the x and y directions are -0.014 ± 0.025(stat.)± 0.33(syst.) mrad and -0.107 ± 0.025(stat.)± 0.37(syst.) mrad, respectively.

We conclude that the neutrino beam intensity and direction remain stable during the measurement based on the precise measurement with INGRID.

References

[1] Z. Maki, M. Nakagawa, S. Sakata, Progress in Theoretical Physics 28 (1962) 870.
[2] B. Pontecorvo, Soviet Physics JETP 26 (1968) 984.
[3] K. Abe, et al., The T2K Experiment, Nuclear Instruments and Methods in Physics Research Section A 659 (2011) 106.
[4] Y. Fukuda, et al., Super-Kamiokande Collaboration, Nuclear Instruments and Methods in Physics Research Section A 501 (2003) 418.
[5] D. Beavis, A. Carroll, I. Chiang, et al., Proposal of BNL AGS E-889, 1995.
[6] K. Matsuoka, et al., Nuclear Instruments and Methods in Physics Research Section A 624 (2010) 591.
[7] K. Abe, , T2K Collaboration, Physical Review Letters 107 (2011) 041801.
[8] A. Pla-Dalmau, A.D. Bross, V.V. Rykalin, gExtruding Plastic Scintillator at Felmilab, h FERMILAB-CONF-03-318-E.
[9] K. Nitta, et al., Nuclear Instruments and Methods in Physics Research Section A 535 (2004) 147.
[10] K.K. Hamamatsu Photonics, Online: ⟨http://www.hamamatsu.com⟩.
[11] M. Yokoyama, et al., Nuclear Instruments and Methods in Physics Research Section A 567 (2010) 622. [arXiv:1007/2712[physics.ins-det]].
[12] H. Kawamuko, T. Nakaya, M. Yokoyama, Proceedings of Science PD07 (2007) 043.
[13] A. Vacheret, S. Greenwood, M. Noy, M. Raymond, A. Weber, in: Nuclear Science Symposium Conference Record, 2007. NSS'07, vol. 3, IEEE, pp. 1984–1991.
[14] GEANT—Detector Description and Simulation Tool, Application Software Group, Computing and Networks Division, CERN, Geneva, 1993.
[15] A. Fcrrari, P.R. Sala, A. Fasso, J. Ranft, CERN-2005-010 and SLAC-R-773 and INFN-TC-05-011, 2005.
[16] G. Battistoni, et al., AIP Conference Proceedings 896 (2007) 31.
[17] C. Zeitnitz, T.A. Gabriel, in: Proceedings of the International Conference on Calorimetry in High Energy Physics, Tallahasse, FL, USA, February 1993.
[18] N. Abgrall, , NA61/SHINE Collaboration, Physical Review C 84 (2011) 034604 arXiv:1102.0983[hep-ex].
[19] T. Eichten, et al., Nuclear Physics B 44 (1972) 333.
[20] Y. Hayato, Nuclear Physics B, Proceedings Supplements 112 (2002) 172.
[21] M. Hasegawa, Ph.D. Thesis, Measurement of Neutrino Oscillation Parameters with Neutrino-Nucleus Interaction Studies in the K2K Experiment. Kyoto University, 2005.
[22] M. Otani, et al., Nuclear Instruments and Methods in Physics Research Section A 623 (2010) 368.
[23] A. Vacheret, T2K Collaboration, Nuclear Instruments and Methods in Physics Research Section A 623 (2010) 201.